Scroll Wave Filaments Terminate in the Back of Traveling Fronts

Tamás Bánsági, Jr., Christine Palczewski, and Oliver Steinbock*

Department of Chemistry and Biochemistry, Florida State University, Tallahassee, Florida 32306-4390

Received: December 7, 2006; In Final Form: January 16, 2007

Experiments with the 1,4-cyclohexanedione Belousov−Zhabotinsky reaction demonstrate that three-dimensional scroll waves can rotate around filaments that end in the wake of a traveling excitation pulse. The vortex structures nucleate during the collision of three nonrotating excitation pulses. The nucleation process and the wave-termination of filaments are direct consequences of the system's anomalous dispersion relation. Vortex filaments are found to expand with about twice the speed of their anchoring wave fronts. Filament expansion is accompanied by the build-up of phase differences in spiral rotation creating strongly twisted wave structures. Experiments employ optical tomography for the reconstruction of the three-dimensional wave patterns.

Introduction

Rotating spiral waves in excitable media are a striking example of self-organization far from thermodynamic equilibrium.[1] These patterns exist in a diverse spectrum of experimental systems such as the Belousov−Zhabotinsky (BZ) reaction, the Briggs−Rauscher reaction, and the oxidation of CO on Pt surfaces.[2] Moreover, many biological systems show spiral waves of excitation including the microorganism *Dictyostelium discoideum*, *Xenopus* oocytes, and cardiac as well as neuronal tissue.[3,4] Most experimental studies of rotating excitation patterns have focused on pseudo-two-dimensional systems such as thin layers of reaction solutions or catalytic surfaces. Under such conditions the main pacemaker of excitation vortices is the spiral tip which, in the simplest case, describes a small circular trajectory around a stationary center.[5] In three-dimensional systems, excitation vortices are typically referred to as scroll waves. Their motion is more complex as rotation occurs around a space curve. The latter curve, known as the filament, can have numerous shapes and spiral motion can vary in phase along the filament leading to twisted patterns.[6]

The dynamics and the topological constraints of filament motion have attracted considerable interest. One important feature is that filaments are believed to end only at the boundaries of the system.[7] Alternatively, the filaments can be closed curves such as simple circles, knots, or chain links.[8] The spatio-temporal evolution of the filament depends on various system parameters. For example, it has been shown that a circular filament can either shrink or expand according to system's filament tension.[9] Shrinkage eventually induces the annihilation of the vortex, and expansion leads to strongly folded filaments and turbulent behavior that is sometimes referred to as Winfree chaos. Moreover three-dimensional excitation vortices are involved in cardiac arrhythmia and sudden cardiac deaths of humans. This important connection has been established in numerous studies that reported excitation vortices in mammalian cardiac tissue and also in mathematical models of the heart.[10] Despite these profound fundamental and biomedical motivations, many aspects of scroll waves remain unclear. In particular, little is known regarding the nucleation of these structures and only sparse experimental data exist on their dynamics.

* To whom correspondence should be addressed. E-mail: steinbck@chem.fsu.edu.

We use the 1,4-cyclohexanedione-Belousov−Zhabotinsky (CHD-BZ) reaction as an experimental model of three-dimensional excitable media.[11] In this system, traveling waves obey an anomalous dispersion relation that has been analyzed in earlier work by our group.[12] The specific anomaly implies that the speed of wave trains increases with decreasing pulse spacing. Consequently, a trailing pulse can travel faster than its predecessor, which induces a "front-to-back" collision. The collision causes the annihilation of the trailing pulse, which explains the, slightly misleading, term "merging" that usually refers to this process. Detailed measurements of the anomalous dispersion relation of merging CHD-BZ waves have been reported in ref 13. We emphasize that this behavior is not simply an isolated feature of this particular chemical reaction medium. Quite to the contrary, qualitatively similar behavior is also found for wave propagation in the catalytic reduction of NO with CO and Pt(100) surfaces, neuronal systems, and numerous reaction-diffusion-type models including models of cardiac tissue.[14,15]

In this Article, we present and analyze three-dimensional reconstructions of merging wave patterns in the CHD-BZ reaction. These data are obtained by optical tomography, a technique that for the detection of chemical waves was first used by Arthur Winfree in the late 1980s.[16] Specifically, we investigate a nucleation mechanism of excitation vortices that is intimately related to the existence of merging waves and demonstrate that the filaments of scroll waves can terminate in the back of traveling pulses. This unexpected finding corrects our current understanding that filaments end only at the system's boundary or close in on themselves. Moreover, we show that the anchoring of filaments to the back of waves causes rapid filament growth and twisting of the scroll wave.

Experimental Section

In this study, the classic organic substrate of the BZ reaction, malonic acid, is replaced by 1,4-cyclohexanedione to create a reaction system with a nonmonotonic dispersion relation. In addition, this substitution prevents the formation of carbon dioxide bubbles that could compromise the spatial homogeneity of the reaction medium. As redox catalyst we employ an organometallic complex of iron and 4,7-diphenyl-1,10-phenanthrolinedisulfonic acid ligands. The complex is referred to as $[Fe(batho(SO_3)_2)_3)]^{3-/4-}$ and acts as a convenient redox indicator with a very large difference between the molar absorption

10.1021/jp068425g CCC: $37.00
Published on Web 03/03/2007

coefficients of the reduced and the oxidized state. The UV/vis absorption spectra of the red, reduced form and the blue, oxidized form are published in ref 17. The stock solution of the catalyst is prepared in 25 mmol/L sulfuric acid by first dissolving 4,7-diphenyl-1,10-phenanthrolinedisulfonic acid (Acros) under vigorous stirring. Then ferrous sulfate heptahydrate (Fluka) is added in a stoichiometric ratio of 3:1 to yield 25 mmol/L of the complex.

The reaction solution is prepared in nanopure water (18 MΩ cm) by mixing stock solutions of $NaBrO_3$ (Fluka), 1,4-cyclohexanedione (CHD, Aldrich), sulfuric acid (Riedel-de Haën, 5 M), $[Fe(batho(SO_3)_2)_3]^{4-}$ (Acros, 25 mM), and polyacrylamide. Disregarding all reactions and accounting for the added polyacrylamide volume, the initial concentrations are $[NaBrO_3] = 0.18$ mol/L, $[CHD] = 0.19$ mol/L, $[H_2SO_4] = 0.60$ mol/L, and $[Fe[batho(SO_3)_2]_3^{4-}] = 0.475$ mmol/L. The volume ratio of aqueous BZ to polyacrylamide solution is 1.8. The addition of polyacrylamide solution prevents hydrodynamic perturbations of the reaction medium by increasing its viscosity from about 1 to 150 mPa s. Notice that the resulting system is *not* a gel. The polyacrylamide stock solution is prepared by first dissolving 20 g of acrylamide (Fluka) in 220 mL of water. Then we add a solution of $(NH_4)_2S_2O_8$, which is prepared by dissolving 0.5 g of $(NH_4)_2S_2O_8$ (Fluka) in 20 mL of water. In the last step, 75 μL of tetramethylethylenediamine (TEMED, Aldrich) is added to initiate polymerization. The very viscous, clear polymer solution forms in about 30 min.

After mixing, 18 mL of the viscous BZ solution is transferred to a cylindrical glass container. The inner diameter and the height of the container are 3.7 and 7 cm, respectively. A rod-shaped, magnetic stir bar is fitted to the bottom of the container. The stir bar can be spun via an external magnetic field. It is used to remix the BZ solution and, thus, remove undesired wave patterns that nucleate spontaneously. Two silver wires are utilized to initiate oxidation waves at predetermined positions. One wire is attached to a microstage and can be lowered to touch the uncovered BZ solution. The second wire is attached to the top of the magnetic stir bar about $r = 1$ mm away from the stir bar's center so that a rotation of angle ϕ will move the silver wire by a distance of $2r \sin(\phi/2) \approx r\phi$. The reaction container is mounted in a setup equipped with an electric motor and a belt drive that allows us to rotate the reaction container steadily around its symmetry axis. This rotation is needed for the specific type of tomography used to reconstruct the three-dimensional wave patterns. The typical rotation frequency is 12.3 rpm. The sample is illuminated with white light from a fiber optics light source (Dolan Jenner Fiber Lite PL-800) through a large area backlight attachment (Dolan Jenner QVABL). A charge-coupled-device camera (Sony XC-75), mounted opposite of the light source, is used to record monochrome views through the rotating sample. Video frames are captured with a PC-based digital frame grabber (Data Translation, DT 3155, 640 × 480 pixels at 8 bit) at a rate of 12.5 frame/s. These parameters imply that 62 frames are recorded during one full rotation of the sample. The spatial resolution is 24.5 pixel/mm and the typical speed of excitation waves in this system is 44 μm/s. Accordingly, the waves move about five pixels during one full rotation and, hence, can be considered near-stationary.

Optical tomography is used to obtain spatially resolved information on the local absorption within the three-dimensional reaction medium. The crucial step in this procedure is to compute the inverse Radon transform of the image data obtained during one complete rotation of the sample. This analysis is carried out using in-house software that employs MATLAB (The MathWorks, Inc., Version 6.5.1) routines. Our tomographic procedure employs "filtered backprojection" and adheres in principle to the descriptions given in refs 16 and 18. The computational scheme relies on the slice-wise reconstruction of the full three-dimensional pattern. For this purpose, the image data I are broken into individual sinograms $I_z(x',\theta)$ where z, x', and θ denote the space coordinate along the vertical rotation axis of the sample, the horizontal space coordinate in each snapshot and the corresponding rotation angle, respectively. Our software computes the desired image $I_z(x,y)$ via (i) backprojection of each sinogram along parallel beams of angle θ and (ii) summation over all θ. Hence,

$$I_z(x,y) \approx \Delta\theta \sum_{\theta} I_z(x \cos\theta + y \sin\theta, \theta)$$

where $\Delta\theta$ specifies the angular resolution of the projections and x and y are real space coordinates perpendicular to the z-axis. The latter equation is refined by filtering the sinogram data in the frequency domain prior to summation. Specifically, we use the Ram-Lak (ramp) filter multiplied by a Hann window, which de-emphasizes high frequencies.

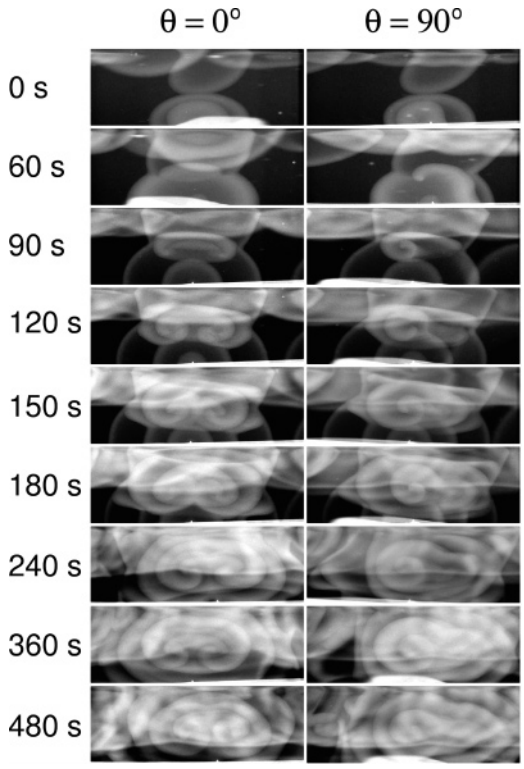

Figure 1. Image sequences illustrating the nucleation and subsequent dynamics of a rotating scroll wave from the collision of three non-rotating wave fronts. The two columns correspond to two different, perpendicular views through the reaction medium. The pictures in each row are recorded nearly simultaneously. Image area of each individual frame: (25.9×9.3) mm^2.

Results

The image sequence in Figure 1 illustrates the nucleation of a three-dimensional scroll wave in the CHD-BZ reaction. The early snapshots in the first row of Figure 1 show that initially the vortex does not exist. However, already 60 s later a spiral-shaped structure is clearly discernible (see right frame of second row). The primary goals of this Article are to explain this nucleation process, to describe the vortex structure, and to

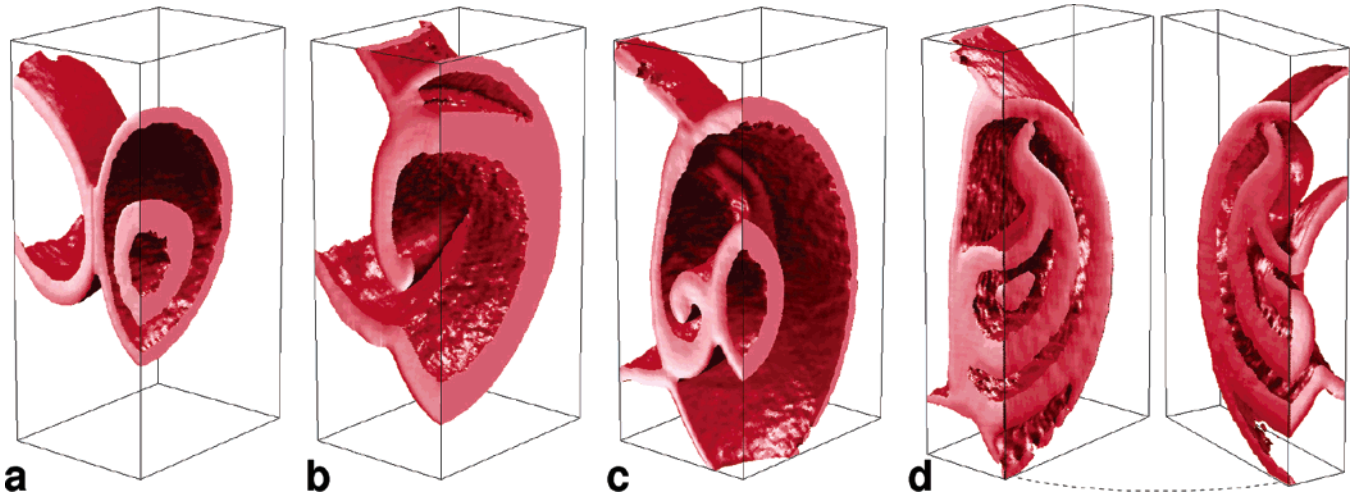

Figure 2. Sequence of four tomographic reconstructions illustrating the nucleation and growth of a rotating scroll wave. The analyzed volume is $(17.2 \times 9.6 \times 6.9)$ mm^3. In (d) the volume is cut into two slices and opened to reveal details of the internal scroll wave structure. The data show the posterior half of the pattern. The omitted anterior halves are essentially mirror images of the patterns shown. The times elapsed between reconstructions (a)−(d) are 60, 30, and 30 s, respectively.

analyze its dynamics. Before we proceed, it is important to briefly discuss how we collect image data and control this interesting nucleation scenario.

As described in the Experimental Section, we monitor the cylindrical sample by rotating it at a steady rate around its symmetry axis. This axis corresponds to the vertical centerline of the image frames. The two columns in Figure 1 present nearly simultaneous snapshots of the wave structure acquired at two different azimuths ($\theta = 0°, 90°$). In this representative example, dark areas correspond to the chemically reduced, and dynamically excitable, rest state of the system. The traveling oxidation pulses are bright bands and most pronounced if the pulse is viewed "tangentially", i.e., in a direction perpendicular to the normal of the pulse front. In addition, local brightness also increases with the number of wave pulses traversed along the corresponding light beam. A good example for the latter, additive effect can be seen around the upper mid-section of the first frame ($\theta = 0°$, $t = 0$ s).

We induce the specific type of wave collision and vortex nucleation shown in Figure 1 by initiating half-spherical wave pulses from thin silver wires. The silver decreases the local concentration of the inhibitory species bromide by formation of an insoluble silver bromide film. One of the two wires is mounted to the top of the stir bar at the bottom of the reaction vessel (not shown) and initiates upward propagating wave pulses at an approximate period of 30 s. The other wire is lowered briefly onto the upper BZ surface and induces only one downward traveling half-sphere. Crucial for this interesting nucleation scenario are exactly three waves, namely two upward propagating and one downward moving pulses. These excitation waves can be discerned easily in the first row of Figure 1. Later, however, they are increasingly obscured by the presence of additional wave patterns that primarily nucleate at the upper, air exposed, surface. These "nuisance" waves appear as white downward moving bands in Figure 1 and affect neither the observed vortex nucleation nor the analyzed vortex dynamics.

The early motion of the three crucial wave fronts induces a collision between the downward moving and the first, upward propagating wave. Because excitation waves show no interference phenomena, this collision creates an hourglass-shaped envelope with an equatorial hole. Due to the anomalous dispersion in our particular system, the trailing, third wave travels faster than its predecessor and vanishes in a front-to-back collision. However, the annihilation of the third pulse is not complete because a small disklike segment survives within the central hole of the hourglass-shaped envelope. In a recent study, we showed that the rim of this disk begins to curl and, thus, becomes a three-dimensional vortex structure that rotates around a circular filament. Moreover, we have shown that twisted scroll rings can be induced by slightly shifting the nucleation site of third wave because this asymmetry tilts the prevortical disk and causes time differences in the onset of rotation.

The experiment in Figure 1 is carried out in a similar fashion but involves a larger displacement of the stir-bar-mounted pacemaker. Notice that this asymmetry can be easily seen in the first row in Figure 1 where the two nested, half-spherical wave fronts at the bottom are clearly not concentric (see right frame). In contrast to our earlier experiments that induced the formation of a twisted scroll ring, the larger displacement causes the nucleation of a qualitatively different structure. The main feature of this vortex can be suspected from the snapshots in the fourth row of Figure 1. The latter frames seem to depict a pair of counter-rotating spirals at an azimuth of $\theta = 0°$ and a single spiral if viewed from a perpendicular direction ($\theta = 90°$). Furthermore, the latter view indicates that the front of the single vortex spirals outward to terminate at the outer hourglass-shaped wave envelope.

Clearly, this description is unsatisfactory and does not reveal the true three-dimensional structure of the vortex. Moreover, the data in Figure 1 show that in the course of time the structure becomes even more complex. We therefore generate tomographic reconstructions of three-dimensional wave pattern with each reconstruction employing not two but 62 different views of the sample. A typical example obtained by optical tomography is given in Figure 2. The figure shows the wave pattern at four different times. The earliest reconstruction (Figure 2a) shows three wave pulses and illustrates the structure during the collision of the two outermost fronts. The trailing, third front is clearly lower than its predecessor. Notice that in Figure 2a−c only the posterior half of the system is shown to provide a more instructive view of the excitation pattern.

The reconstruction in Figure 2b describes the pattern 60 s later and shows the newly formed spiral rotor as a hook-like structure in the foreground. For the given perspective, rotation occurs in counter-clockwise direction. The main surface of the

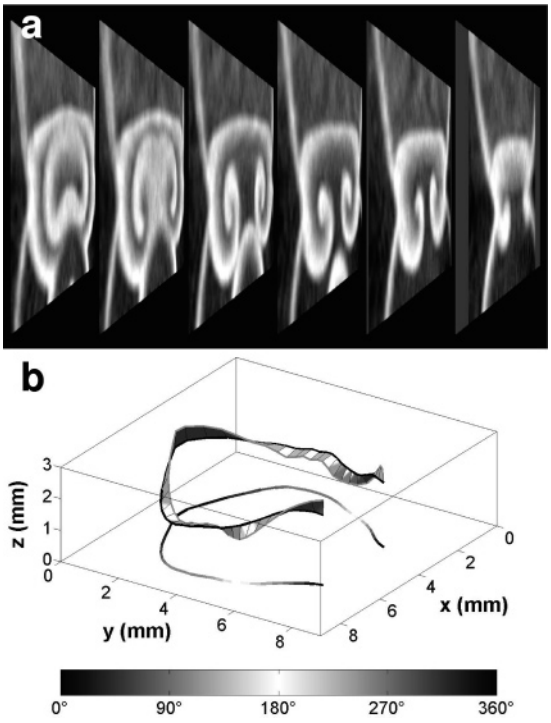

Figure 3. (a) Six equidistant slices obtained from a tomographically reconstructed volume snapshot. The spacing between the slices is 1.3 mm. The perspectively deformed frames show an area of (15.9 × 6.9) mm^2. (b) The filament of the wave pattern in (a) is plotted as the thick, black space curve. The accompanying ribbon structure represents the phase of spiral rotation along the filament. The filament itself is also projected into the *xy* plane where the local phase is encoded as gray levels according to the scaling bar.

spiral is the remainder of the trailing, third wave in Figure 2a. Apparently, its upper portion failed to detach and its lower part created a slightly curved filament that spans the interior of outer wave envelope. This filament essentially traces the rim of the spiral in (b). The third reconstruction (Figure 2c) shows the same vortex about three-quarters of a rotation period later. The filament remains anchored at the back of the outermost pulse but is now more curved than in (b). Parts of the filament are hidden behind a newly formed spherical wave that nucleated at the stir-bar-mounted silver wire. During its subsequent evolution the scroll wave becomes more and more convoluted. In Figure 2d, we therefore cut the volume further and open up the two resulting volume slices. The interior wave pattern appears to be twisted and its filament has become s-shaped. We re-emphasize that the reconstructions in Figure 2 depict the posterior half of the wave pattern. The hidden anterior half is essentially the mirror image of the displayed volume.

To obtain further insights into the shape and dynamics of the wave structure, we extract the filament from the tomographically reconstructed, three-dimensional wave patterns. For this analysis, we typically cut the pattern into two-dimensional slices and record the positions and the phases of spiral tips. The latter values are angles that represent the tip directions in planes perpendicular to the filament. Figure 3a shows six equidistant slices across the scroll wave. Notice that these image data are not raw images but true two-dimensional slices of the three-dimensional absorption pattern. The first image frame on the left corresponds to the turning point of the filament, and the sixth frame depicts a cut close to the terminal points of the filament. Closer inspection of the data in Figure 3a reveals that the phase of spiral rotation is not constant across the different slices. Figure 3b quantifies these observations by plotting a ribbon representation of the filament. In this diagram, the filament itself is plotted as a thick black curve and the rotation phase is represented by the direction of the ribbon wall. In addition, the curve is projected into the *xy* plane where the phase is now encoded as different gray levels according to the scaling bar below.

The data in Figure 3 show that the scroll wave twists and detwists as one moves along the filament. Moreover, the filament is not strictly planar. In the example shown, it extends about 6.5 mm in the *x* and *y* directions and wiggles approximately 1 mm in the *z* direction. Figure 4a illustrates the temporal evolution of the filament by presenting the filaments' projections into the *xy* plane. Here, gray levels do not denote local rotation phases but simply help distinguish the curves obtained at different times. Over a period of 150 s, which corresponds to approximately three and a half vortex rotations, the filament's apex is essentially stationary. The two (horizontal) sides are clearly undulated due to a slightly helical shape in three dimensions. These "wiggles" are not stationary but move as the overall filament expands in an overall *y* direction.

The growth in filament length is closely related to the anchoring of the filament to the back of a traveling wave pulse. Figure 4b analyzes the total filament arclength as a function of time. The presented data are obtained from two representative experiments. Within the analyzed time interval, the filament length increases linearly with time yielding constant growth rates of (0.11 ± 0.01) mm/s (squares) and (0.09 ± 0.01) mm/s (circles) for the two data sets in Figure 4b. Both rates are very similar to the 2-fold propagation speed of the outer wave front, which we measured as (0.044 ± 0.002) mm/s. This finding suggests that filament expansion occurs primarily from the motion of the filament's two terminal points, which each move at a speed that equals the velocity of the anchoring wave back. Furthermore, the result indicates the absence substantial filament elongation at other positions.

The three-dimensional reconstruction of the initial scroll in Figure 2b reveals only a very small phase differences, while the ribbon plot of the more mature pattern in Figure 3d shows a pronounced twisting. Hence, the underlying phase differences must increase during the course of vortex rotation and filament expansion. We note that this behavior is qualitatively different from the dynamics of twisted scroll *rings*, which for very similar conditions were shown to untwist rapidly.[19] Figure 4c quantifies the twisting process by plotting the rotation phase ϕ as a function of filament arclength *s* for a typical scroll wave pattern. The analysis is carried out for five different times during the first 4 min of vortex rotation. For all five data sets, the rotation phase at $s = 0$ is set to zero. We find that the phase increases along the filament to reach a maximum at about half the filament length. After passing the maximum, the values return to nearly zero indicating that spiral rotation at the two terminal points is essentially in phase.

The earliest measurement in Figure 4c (circles) yields phase data that vary between 0° and about 210° along a still rather short, 14 mm long filament. The subsequent data sets document that the maximum phase difference increases continuously in the course of time. The last measurement in Figure 4c (upward triangles) shows phase variations of about 540° and qualitative inspection of later image data (not shown) suggests that the scroll wave continues to twist in the course of its expansion. Another interesting feature of the results in Figure 4c concerns the values of $d\phi/ds$. Despite some minor shoulder-like features, our results seem to suggest a characteristic value of $|d\phi/ds| =$

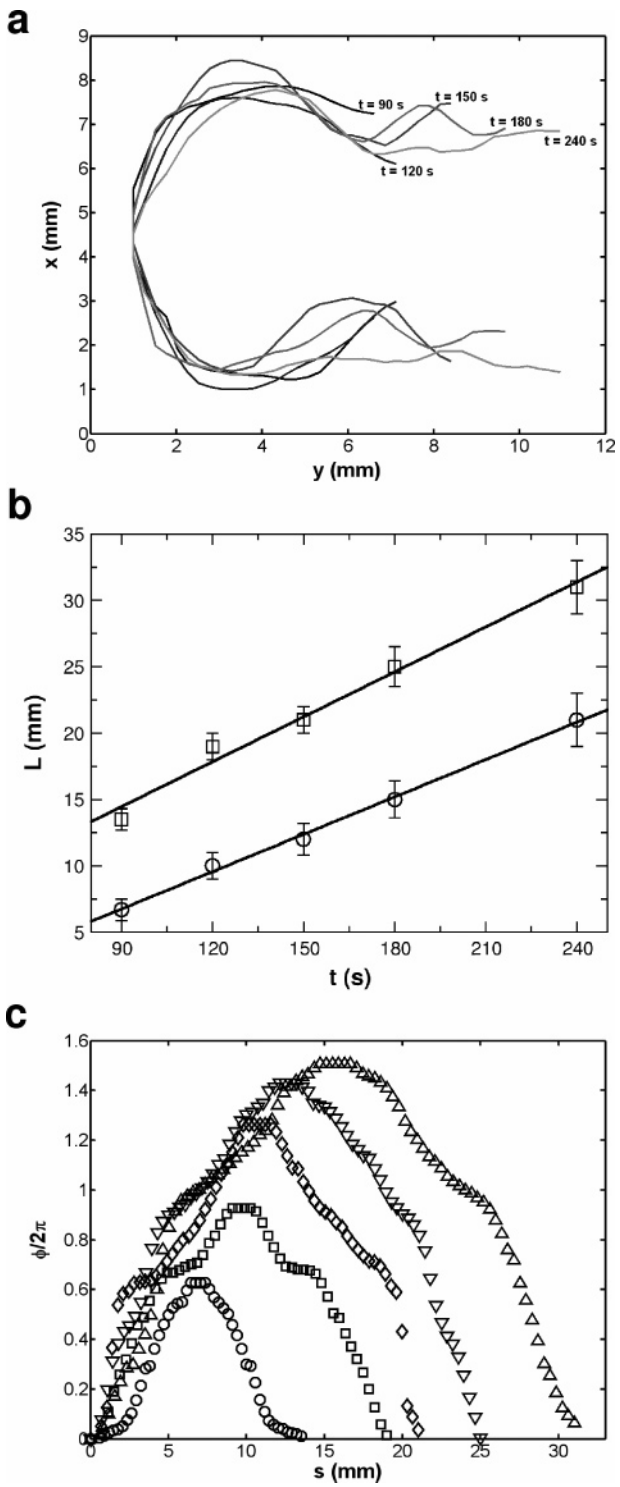

Figure 4. (a) Projections of a scroll wave filament into the *xy* plane. Each projection is obtained at a different time as indicated by the values in the diagram. The ends of the filament curves correspond to the filament's terminal points in the wake of the surrounding, non-rotating excitation pulse. (b) Total arclength L of a filament as a function of time as obtained from two typical experiments that differed mainly in the curvature of the initial arch-shaped filament. The straight lines represent the best linear fits. (c) Phase of spiral rotation ϕ as a function of filament arclength s. The results are obtained from the same experiment as the data values shown as squares in (b). The individual symbols in (c) correspond to the following times: 90 s (circles), 120 s (squares), 150 s (diamonds), 180 s (downward triangles), and 240 s (upward triangles).

0.67 rad/mm within the flanks of $\phi(s)$. Unfortunately, it is unclear whether the asymptotic behavior of $\phi(s)$ is truly linear.

Discussion and Conclusions

The experiments described in this Article are characterizing a novel nucleation mechanism of three-dimensional scroll waves. The nucleation process involves neither stationary nor temporary obstacles at which wave pulse could break to create spiral rotation.[20] Quite contrary, it occurs under spatially homogeneous conditions and arises from simple wave collisions that are copious in excitable systems. However, this novel type of vortex nucleation is likely to be limited to systems with anomalous dispersion relations, i.e., systems in which trailing excitation pulses can propagate faster than their immediate predecessor. We emphasize that this so-called anomaly has been reported for many theoretical models as well as several experimental systems.[12−15] It is therefore likely that the nucleation mechanism should be observable in variety of physical, chemical and biological media.

Our studies show that the nucleation scenario's quintessential ingredients are three non-rotating waves of which one must be fully enclosed by one of the others (cf. Figure 2a). If this three-wave constellation leads to a front-to-front and a subsequent front-to-back collision, a variety of three-dimensional vortices can nucleate. These structures include untwisted and twisted scroll rings, as shown in an earlier paper,[19] as well as scroll waves with noncircular filaments as shown here. Among those three cases, pattern selection is intricately related to the location of the nucleation center of the third, i.e., the trailing and vortex-forming, wave front as well as the timing of its annihilation. Although the details of the selection process are not fully understood yet, one crucial parameter seems to be the distance d between the nucleation site of the third wave and the line connecting the two other nucleation centers. Untwisted scroll rings form only for the case of $d = 0$. Twisted scroll rings nucleate for nonzero, but small values of d and the noncircular filaments, analyzed in this Article, occur only for sufficiently large d. We believe that additional measurements and more importantly theoretical analyses are needed to obtain a quantitative understanding of the rules that govern the striking difference between the nucleation of circular and noncircular vortex filaments.

Perhaps the most important result of our study is that vortex filaments do not terminate at system boundaries! Our results unequivocally demonstrate that the filaments of three-dimensional excitation vortices can end in the wake of moving wave fronts. This observation is of fundamental importance because it extends our current understanding of the topological constraints that govern the basic characteristics of scroll wave filaments. Moreover, a wave-terminated filament is dynamically more interesting because its terminal points are nonstationary. As we have shown here, one of the consequences of wave termination is the steady growth of the phase differences along the expanding filament. To our knowledge this result is the first experimental report of increasing phase-differences in a homogeneous, gradient-free medium. The driving force behind this phenomenon is the particular refractory profile in the wake of the filament-terminating wave pulse. As the system's dispersion relation is anomalous, it is very likely that spiral rotation close to the filament's termini is faster than along the filament's midsection. On the basis of this frequency difference, we conclude that the twisting is driven from the end points only. The factors opposing the steady buildup of phase gradients are the filament expansion and the natural tendency of the pattern to untwist. In addition, our measurements show helical deformations of the filament that are likely to be the consequence of the steady twisting. It is reasonable to assume that at later stages

the filaments undergo additional coiling to form even more complex structures.[21] It is also conceivable that the resulting superhelices could break into individual segments as they collide with their wave envelope.

The finding of wave-terminated filaments generates a whole host of new questions. For example, we do not understand the long-term dynamics of the filament in response to its continuous twisting and elongation by the expanding wave envelope. Another puzzling question concerns the response of wave-terminated filaments to the annihilation of their anchoring wave pulse; a situation that can easily arise in a front-to-front collision with another excitation pulse. Obviously, more work is needed to answer these intriguing questions and evaluate their relevance to biological systems. We believe that future activities will benefit from additional experiments on vortex dynamics in the CHD-BZ reaction because it is a very good model for this generic class of excitable media. Such experimental work, however, will always be limited by the finite lifetime of the closed reaction medium as the construction of continuously fed three-dimensional reactors seems to be impossible. Hence, future studies of vortices in the CHD-BZ reaction will have to be complemented by theoretical and numerical investigations.

Acknowledgment. This material is based upon work supported by the National Science Foundation under Grant No. 0513912.

References and Notes

(1) Rabinovich, M. I.; Ezersky, A. B.; Weidman, P. D. *Dynamical Theory of Pattern Formation*; World Scientific: Singapore, 2000.

(2) Kapral, R., Showalter, K., Eds. *Chemical Waves and Patterns*; Kluwer: Dordrecht, The Netherlands, 1995.

(3) (a) Goldbeter, A. *Biochemical Oscillations and Cellular Rhythms*; Cambridge University Press: Cambridge, U.K., 1996. (b) Müller, S. C.; Mair, T.; Steinbock, O. *Biophys. Chem.* **1998**, *72*, 37−47.

(4) (a) Lechleiter, J.; Girard, S.; Peralta, E.; Clapham, D. *Science* **1991**, *252*, 123−126. (b) Davidenko, J. M.; Pertsov, A. V.; Salomonsz, R.; Baxter, W.; Jalife, J. *Nature* **1992**, *355*, 349−351. (c) Gorelova, N. A.; Bures, J. *J. Neurobiol.* **1983**, *14*, 353−363.

(5) (a) Winfree, A. T. *Chaos* **1991**, *1*, 303−334. (b) Barkley, D. *Phys. Rev. Lett.* **1994**, *72*, 164−167.

(6) Wellner, M.; Berenfeld, O.; Jalife, J.; Pertsov, A. M. *Proc. Natl. Acad. Sci. U.S.A.* **2000**, *99*, 8015−8018.

(7) Pertsov, A. M.; Wellner, M.; Vinson, M.; Jalife, J. *Phys. Rev. Lett.* **2000**, *84*, 2738−2741.

(8) Sutcliffe, P. M.; Winfree, A. T. *Phys. Rev. E.* **2003**, *68*, 016218. Keener, J. J.; Tyson, J. P. *SIAM Rev.* **1992**, *34*, 1−39.

(9) (a) Alonso, S.; Sagues, F.; Mikhailov, A. S. *J. Phys. Chem A* **2006**, *110*, 12063−12071. (b) Zaritski, R. M.; Mironov, S. F.; Pertsov, A. M. *Phys. Rev. Lett.* **2004**, *92*, 168302. (c) Alonso, S.; Sagues, F.; Mikhailov, A. S. *Science* **2003**, *299*, 1722−1725.

(10) (a) Fenton, F. H.; Cherry, E. M.; Karma, A.; Rappel, W. J. *Chaos* **2005**, *15*, 013502. (b) Jalife, J. *Ann. Rev. Physiol.* **2000**, *62*, 25−50. (c) Winfree, A. T. *Science* **1973**, *181*, 937−939.

(11) (a) Kurin-Csörgei, K.; Szalai, I.; Molnár-Perl, I.; Körös, E. *React. Kinet. Catal. Lett.* **1994**, *53*, 115−121. (b) Kurin-Csörgei, K.; Zhabotinsky, A. M.; Orbán, M.; Epstein, I. R. *J. Phys. Chem.* **1996**, *100*, 5393−5397. (c) Szalai, I.; Körös, E.; Györgyi, L. *J. Phys. Chem. A.* **1999**, *103*, 243−249.

(12) (a) Manz, N.; Steinbock, O. *Chaos* **2006**, *16*, 037112. (b) Manz, N.; Steinbock, O. *J. Phys. Chem. A* **2004**, *108*, 5295−5298. (c) Müller, S. C.; Manz, N.; Steinbock, O. *J. Phys. Chem. A* **2000**, *104*, 5895−5897.

(13) Hamik, C. T.; Manz, N.; Steinbock, O. *J. Phys. Chem. A* **2001**, *105*, 6144−6153.

(14) Christoph, J.; Eiswirth, M.; Hartmann, N.; Imbihl, R. Kevrekidis, I. G.; Bär, M. *Phys. Rev. Lett.* **1999**, *82*, 1586−1589.

(15) (a) Elphick, C.; Meron, E.; Spiegel, E. A. *Phys. Rev. Lett.* **1988**, *61*, 496−499. (b) Bordiougov, G.; Engel, H. *Physica D* **2006**, *215*, 25−37. (c) Falcke, M.; Or-Guil, M.; Bär, M. *Phys. Rev. Lett.* **2000**, *84*, 4753−4756.

(16) Winfree, A. T.; Caudle, S.; Chen, G.; McGuir, P.; Szilagyi, Z. *Chaos* **1996**, *6*, 617−626.

(17) Ginn, B. T.; Steinbock, B.; Kahveci, M.; Steinbock, O. *J. Phys. Chem. A* **2004**, *108*, 1325−1332.

(18) (a) Storb, U.; Neto, C. R.; Bär, M.; Müller, S. C. *Phys. Chem. Chem. Phys.* **2003**, *5*, 2344−2353. (b) Deans, S. R. *The Radon Transform and Some of Its Applications*; Wiley: New York, 1983. (c) Kak, A. C.; Slaney, M. *Principles of Computerized Tomographic Imaging*; IEEE Press: New York, 1988.

(19) Bánsági, T., Jr.; Steinbock, O. *Phys. Rev. Lett.* **2006**, *97*, 198301.

(20) (a) Welsh, B. J.; Gomatam, J. *Physica D.* **1990**, *43*, 304−317. (b) Luengviriya, C.; Storb, U.; Hauser, M. J. B.; Müller, S. C. *Phys. Chem. Chem. Phys.* **2006**, *8*, 1425−1429.

(21) Rousseau, G.; Chate, H.; Kapral, R. *Phys. Rev. Lett.* **1998**, *80*, 5671−5674.